Published in final edited form as:
Dev Biol. 2013 January 15; 373(2): 373–382. doi:10.1016/j.ydbio.2012.10.024.

Negative regulation of *Shh* levels by *Kras* and *Fgfr2* during hair follicle development

Anandaroop Mukhopadhyay, **Suguna Rani Krishnaswami**, **Christopher Cowing-Zitron**, **Nai-Jung Hung**, **Heather Reilly-Rhoten**, **Julianne Burns**, and **Benjamin D. Yu**[*]
Division of Dermatology, Department of Medicine, Institute for Genomic Medicine, Stem Cell Program, University of California, San Diego, CA 92093, USA

Abstract

Activating mutations in the *KRAS* oncogene are associated with three related human syndromes, which vary in hair and skin phenotypes depending on the involved allele. How variations in RAS signals are interpreted during hair and skin development is unknown. In this study, we investigated the developmental and transcriptional response of skin and hair to changes in RAS activity, using mouse genetic models and microarray analysis. While activation of *Kras* ($Kras^{G12D}$) in the skin had strong effects on hair growth and hair shape, steady state changes in downstream RAS/MAPK effectors were subtle and detected only by transcriptional responses. To model the transcriptional response of multiple developmental pathways to active RAS, the effects of growth factor stimulation were studied in skin explants. Here FGF acutely suppressed *Shh* transcription within 90 minutes but had significantly less effect on Eda, WNT, Notch or BMP pathways. Furthermore, *in vivo Fgfr2* loss-of-function in the ectoderm caused derepression of *Shh*, revealing a role for FGF in *Shh* regulation in the hair follicle. These studies define both dosage sensitive effects of RAS signaling on hair morphogenesis and reveal acute mechanisms for fine-tuning *Shh* levels in the hair follicle.

INTRODUCTION

RAS is a common downstream component of multiple signaling pathways, which include receptor tyrosine kinases (RTKS), associated growth factors, cytokines, integrin cross-linking, G-protein coupled receptors activation, and other stimuli (Reuther and Der, 2000). In its active state, RAS stimulates several parallel effector pathways, and depending on the experimental setting, a variety of cellular responses may ensue including migration, proliferation, survival, differentiation, and senescence (Malumbres and Barbacid, 2003; Rodriguez-Viciana et al., 1997). In the setting of cancer, mutations in RAS maintain RAS in its activated state and drive persistent proliferation and survival of transformed cells via one or more effector pathways. As a central mediator of multiple signaling pathways, pharmacologic inhibition of RAS, its post-translational modification, or its downstream effector proteins has been widely pursued as a potential treatment for cancer (Bollag et al., 2010; Downward, 2003; Rodriguez-Viciana et al., 2005).

Mutations in RAS paralogs are also found in a growing number of genetic disorders, including Costello, Cardiofaciocutaneous and Noonan syndromes (Rauen et al., 2010; Tidyman and Rauen, 2009). Collectively, these syndromes, termed RAS/MAPK syndromes or RASopathies, manifest in patients with several developmental abnormalities including craniofacial, cardiac, neural, cognitive and ectodermal defects. Cardiac defects include

[*]To whom correspondence should be addressed: Benjamin Yu, UCSD School of Medicine, 9500 Gilman Dr., MC-0869, La Jolla, CA 92093-0869, Telephone:858-534-9426, Fax: 858-534-9425, byu@ucsd.edu.

valvular malformations, cardiac hypertrophy, and arrhythmias (Lin et al., 2011), and in the nervous system, patients are affected by delayed development, cerebellar enlargement and cognitive defects (Axelrad et al., 2009; Gripp et al., 2010). In the integument, epidermal, hair, and nail defects are more divergent among RAS/MAPK syndromes. In Costello syndrome, redundant skin, papillomas, and palmar defects are highly characteristic, while sparse hair and perifollicular changes are common and characteristic in CFC patients (Siegel et al., 2012). Other phenotypes, including curly hair and heat intolerance, are common to both CFC and Costello syndrome. Differences in skin phenotypes provide important criteria for delineating between the three distinct syndromic forms (Siegel et al., 2011).

Cutaneous phenotypes among RAS/MAPK syndromes suggest that different RAS paralogs, alleles and effectors are capable of inducing distinct developmental responses. In Costello syndrome (CS), patients (>95%) carry activating *HRAS* mutations (Aoki et al., 2005); CFC patients (~60%) show predominantly *BRAF*, *MEK1*, or *MEK2* mutations (Rodriguez-Viciana et al., 2006); 50% of Noonan syndrome patients carry *PTPN11* loss-of-function mutations (Noonan, 2006). Uncommonly, mutations in the paralog *Kras* occur in RAS/MAPK syndromes. Mutations of this paralog have been reported in all three syndromes, including *KRAS*[K5E/K5N/F156L] in CS (Bertola et al., 2007; Zenker et al., 2007) and *KRAS*[P34R/V14I/T58I/D153V] in CFC/Noonan (Schubbert et al., 2006). The pleiotropic effects of *KRAS* mutations indicate that that paralog differences alone may not be sufficient to explain the phenotypic spectrum of RAS/MAPK syndromes. Moreover, in mouse models, when $Kras^{G12D}$ is activated in the skin, KRAS causes redundant skin, hair loss and papillomas, which are characteristics features of *HRAS*-associated Costello syndrome in humans (Mukhopadhyay et al., 2011). These studies suggest that phenotypic variation in the skin may be caused by both allelic differences and paralog differences in RAS/MAPK syndromes.

Differential cellular responses to RTK signal strength has been implicated as a mechanism to specify multiple cell fates and developmental responses using a single signaling pathway (Schweitzer and Shilo, 1997). In experimental models, amplitude and duration of RTK activation contribute to differential cellular and discrete transcriptional responses (Marshall, 1995; Murphy et al., 2002). The spectrum of phenotypes that differentiate RAS/MAPK syndromes suggest developmental dose-sensitive RTK responses may also exist in the hair and skin of humans and other mammals. To identify developmental and signaling mechanisms that sense changes in RAS activity, we sought to identify RAS-responsive molecular and developmental pathways in the skin using a $Kras^{G12D}$ gain-of-function model. In this model, $Kras^{G12D}$ allele induced a curly hair phenotype, altered hair shaft features important for the production of hair subtypes, and altered the transcriptional program of several developmental pathways of the hair follicle. To identify developmental pathways that are sensitive to RAS signal strength, the transcriptional response of skin explants was examined in response to varying doses of growth factors and inhibitors of the RAS signaling pathway. This approach revealed that growth factor stimulation acutely downregulates *Shh* in the hair follicle. These studies provide evidence for the sensitivity of developmental pathways of the skin in response to RAS signal variation.

MATERIALS AND METHODS

Mice and animal care

Mice have been generated and genotyped as previously described for $Kras^{tm4Tyj}$/J (Tuveson et al., 2004) and $Fgfr2^{flox/flox}$ alleles (Yu et al., 2003). Lines have been maintained in mixed genetic backgrounds. All experiments were performed according to the institutional guidelines established by the University of California, San Diego, Institutional Animal Care and Use Committees.

Analysis of hair, hair length, and hair shaft structures

Hair shafts were plucked from three P14 and three P47 animals from each genotype: wildtype and *Msx2*-cre; *Kras*^{G12D} mice. The numbers of bends and medullar spaces were tabulated as independent features. Statistical analysis was performed with Prizm 5 (GraphPad Software).

Hair length was determined using Image (Wayne Rasband, NIH) and the distributions of hair lengths were compared using the Kendall-Sherman test. For analysis of hair growth from P4 to P7, fixed skin was dehydrated in ethanol and cleared in methyl salicylate. Thick sections (2–3 hair follicles wide) were cut, imaged, and analyzed by NeuronJ (Meijering et al., 2004). Cuticle casts were generated from imprints of hair shafts, embedded in Permount and air-dried overnight at room temperature.

Protein phosphorylation analysis

Dorsal skin from postnatal (P) day 7 wildtype and *Msx2*-cre; *Kras*^{G12D} mice was collected, minced, frozen, and pulverized in liquid nitrogen. Protein was isolated in lysis buffer containing 50 mM TrisHCl (pH 7.5), 150 mM NaCl, 1% NP-40, 0.25% sodium deoxycholate, 1 mM EDTA, 5 mM NaF, 2 mM sodium vanadate, and 1x Complete protease inhibitor (Roche). Antibodies used in Western blotting are listed in Supplementary Methods. Western analysis was performed with goat anti-mouse IgG (IRDye 800CW, Li-COR, USA) and goat anti-rabbit IgG (IRDye 680CW, Li-COR, USA), visualized using an Odyssey Infrared Imager (Li-COR, USA).

Gene expression analyses, real-time PCR and microarray studies

Dorsal skin where Msx2-cre is most active was used for RNA studies. Whole skin was minced, transferred into TRIzol (Life Technologies Corp.), and homogenized by mechanical bead disruption (BioSpec Products). Total RNA was isolated according to manufacturer's protocol. Quantitative RT-PCR was performed using Maxima qPCR reagents (Fermentas Inc.) and a LightCycler 480 (Roche). Taqman reagents and primers for SYBR reactions are listed in Supplementary Methods. Relative mRNA levels were normalized to beta-actin and expressed using a baseline-independent method was used to determine the fractional cycle number and the cycle number was used to calculate the amount of each product using the delta CP calculations. Levels of PCR product were expressed as a function of beta-actin.

Microarray analysis was performed in triplicate from total RNA of control and *Msx2*-cre; *Kras*^{G12D} P7 mice by the UCSD BIOGEM Microarray core for quality control, reverse transcription, labeling, and hybridization to Mouse WG-6 V2 Beadchips (Illumina, Inc.). Differential gene expression p-values were calculated from multiple hypothesis correction (Yekutieli and Benjamini, 2001). For comparison of microarray data to hair follicle lineages, we used the standards described in GEO Dataset GDS1323 (Rendl et al., 2005) to determine cell-type specific genes, as defined by ≥ 2-fold in one cell population as compared to all others. Additional statistical methods are detailed in Supplemental methods. Wildtype and *Msx2*-cre; *Kras*^{G12D} mouse skin microarray data can be accessed at the ArrayExpress database, accession: E-MTAB-700.

Histology, *in situ* hybridization, and immunofluorescence staining

Histology was performed as previously described (Mukhopadhyay et al., 2011). *In situ* hybridization was performed as previously described (Etchevers et al., 2001). Anti-sense digoxygenin riboprobes were generated, according to manufacturer's instructions (Roche). *K17* riboprobe was generated from a PCR template using forward (5'-TGGCAGTGGTTATGGAGGCAAC-3') and reverse primers (5'-CCAGCAATCCTACCTTGTTCTTCAG-3') containing T7 promoter. *Shh* riboprobe was

previously described (Lewis et al., 2001). Image capture was performed with a DP71 (Olympus) camera mounted on a BX51 stereomicroscope (Olympus).

Immunofluorescence staining was performed on paraformaldehyde-fixed tissue in conjunction with citrate antigen retrieval. Primary antibodies used were: phospho-H3 (Ser10) (1:250, Cell Signaling), AE15 (1:500, Santa Cruz Biotechnologies), AE13 (1:500, Santa Cruz Biotechnologies).

For cell counts, positive phospho-H3 and *Shh* staining in hair follicles were counted from at least three mice and subjected to a Mann-Whitney statistical test from Prism 5 (GraphPad Software, Inc.)

Skin explant culture and analysis

Wildtype 1.5 mm punch biopsies were obtained from the dorsal skin of euthanized CF1 outbred and C576Bl/6 inbred P7 animals and placed in DMEM supplemented with 10% fetal calf serum (Mediatech, Inc.) and antibiotics. Growth factors and their sources are provided on Supplemental Methods. Explants were treated with vehicle, media and serum for 90 minutes were used as controls. RNA was extracted from biopsies as above and analyzed by quantitative RT-PCR.

RESULTS

RAS gain-of-function alters hair shape and size

In order to activate $Kras^{G12D}$ from its endogenous locus, we utilized a *loxP* permissive allele, *LSL-*$Kras^{G12D}$, in which a *loxP*-STOP-*loxP* (*LSL*) cassette prevents gene expression until excised by Cre recombinase. To perform Cre-*loxP* recombination in the hair follicle, we bred *LSL-*$Kras^{G12D}$ mouse to the *Msx2*-cre transgenic line, which is active in the matrix of the postnatal hair follicle and in the dorsal skin during embryonic development (Pan et al., 2004; Sun et al., 2000). In other embryonic tissues, *Msx2*-cre is expressed in the apical ectoderm ridge of the early limb bud. Offspring carrying both *Msx2*-cre and *LSL-*$Kras^{G12D}$ (hereafter referred to *Msx2*-cre; $Kras^{G12D}$) were viable and lacked obvious external changes, e.g. normal limbs and facies. Thus, *Msx2*-cre overcomes the neonatal lethality associated with previously reported activation of $Kras^{G12D}$ by keratinocyte-specific *Keratin 14* (*K14*)-cre (Tuveson et al., 2004).

Hair growth in *Msx2*-cre; $Kras^{G12D}$ became visibly abnormal by 1–2 weeks (Fig. 1A). Mice produce four different hair types, guard, awl, auchene and zigzags, which can be identified based on differences in their length, relative frequency, number of constrictions (bends), and internal columns (medulla) (Mustonen et al., 2003; Sundberg, 1994). Microscopic analysis of *Msx2*-cre; $Kras^{G12D}$ hair revealed multiple abnormalities in hair shaft formation (Fig. 1B). Hair bends were absent in *Msx2*-cre; $Kras^{G12D}$ mice. In addition, the number of medulla per hair ($P = 0.004$; ANOVA) and length ($P=1.7 \times 10^{-12}$; ANOVA) were reduced in *Msx2*-cre; $Kras^{G12D}$ mice (Fig. 1C). To characterize the short hair phenotype, we examined hair length at P4 and P7 of cleared whole skin (Fig. 2A). Image tracings of hair from wildtype skin demonstrated an average of 1.81 mm growth over the three-day period, while *Msx2*-cre; $Kras^{G12D}$ littermates grew only 0.82 mm within the same interval (Fig. 2B–D). These findings indicate that the reduced hair length of *Msx2*-cre; $Kras^{G12D}$ mice is caused by slower hair growth.

To investigate other possible causes of short hair, we examined the timing of hair development in *Msx2*-cre; $Kras^{G12D}$ mice. The earliest hair follicles of the dorsal skin initiate development at embryonic (E) day 14.5 and are responsible for the production of the longest hairs (guard hairs). We assessed that presence of hair follicles at E15.5 by the

expression of keratin 17 (*K17*) and found that placode maturation and density was normal in *Msx2*-cre; *Kras*^{G12D} embryos (Fig. 3A). At neonatal and early postnatal stages, when all hair types are present, hair follicles were identified at normal density and maturation (Fig. 3B, C; Suppl. Fig. S2). In addition, differentiation into hair shaft lineages, medulla, cortex and cuticle, was readily detected (Fig. 3D, E). Further analysis of the external morphology of *Msx2*-cre; *Kras*^{G12D} hair shafts showed normal cuticle morphology (Suppl. Fig. S2). To investigate the reduced hair production of *Msx2*-cre; *Kras*^{G12D} mice, proliferation of the hair matrix was examined (Fig. 3F, G). The number of phospho-histone H3-positive cells in the hair follicle bulb region, a molecular change equivalent to mitotic index, was significantly reduced in *Msx2*-cre; *Kras*^{G12D} mice (P=0.03). These findings indicate the activated RAS does not specifically block hair differentiation but alters the rate of hair growth.

Cutaneous activation of RAS induces genes associated with the RTK-signaling pathway

The *Kras*^{G12D} allele, while acting as a gain-of-function, has been shown to be hyperactive rather than persistent and constitutive in other models (Tuveson et al., 2004). To determine if the steady-state level of RAS activation was normal in the skin of *Msx2*-cre; *Kras*^{G12D} mice, we examined the overall activity of the RAS/MAPK pathway at P7 by a quantitative, non-enzymatic Western approach (Fig. 4A, B). In addition, whole skin was utilized as extensive dissection of tissue would likely lead to non-physiologic activation of the RAS/MAPK pathway. Levels of phosphorylated MEK, ERK and AKT were found to be normal in the *Msx2*-cre; *Kras*^{G12D} mice.

Although *Kras*^{G12D} is active and sufficient to induce phenotypic changes in the hair, epigenetic events such as the upregulation of negative feedback networks may reset the steady state levels of phosphorylated downstream proteins *in vivo* (Courtois-Cox et al., 2006). Because multiple RAS/MAPK antagonists are transcriptionally-induced in response to growth factor stimulation, their expression was used as a transcriptional signature of elevated RAS/MAPK signaling (Kawakami et al., 2003; Verheyden et al., 2005). Extensive dissection of hair follicles and injury potentially activate RAS/MAPK ectopically (Corson et al., 2003). To reduce the likelihood of ectopic activation, whole skin of P7 animals was used as a source for RNA with the caveat that some changes in hair follicle gene expression may be diluted by surrounding tissue. Extracted RNA was subjected to microarray hybridization analysis, interrogating 45,281 unique, expressed transcripts of 18,122 genes (Fig. 5). Microarray analysis revealed 1,891 significantly altered genes (≥25% change from wildtype, with P<0.05) and 144 genes altered by greater than 2-fold (Fig. 5A). Affected genes in *Msx2*-cre*; Kras*^{G12D} mice included RAS/MAPK antagonists and other biomarkers of RAS/MAPK activation, e.g. Ets variant transcription factors, *Etv1*, and *Etv4*, *Etv5*, *Dusp6* and others (Fig. 5B). For several genes, real-time PCR was performed to confirm the altered quantities of these transcripts (Fig. 5C). These studies confirmed that the *Msx2*-cre; *Kras*^{G12D} skin represents a heightened level of RAS/MAPK signaling and suggested that in a developmental steady state, the developmental and transcriptional response to RAS gain-of-function may be more sensitive than biochemical changes.

Effects of *Kras*^{G12D} on hair proliferation and differentiation

RAS gain-of-function also had significant effects on hair signaling and gene expression. A comparison of *Kras*^{G12D}-affected genes with hair lineage gene expression (Rendl et al., 2005) revealed repression of hair matrix lineage genes, including many involved with ectodermal development and proliferation (Fig. 5D). In adjacent tissues, genes expressed by the adjacent dermal papilla were not significantly altered and upregulated in the outer root sheath. Lineage gene expression changes indicate that RAS has selective effects on hair follicle lineages. The downregulation of matrix-specific genes and positive regulators of

proliferation led us to study the effect of *Kras*^{G12D} on lineage differentiation and cell proliferation of the hair follicle (Fig. 5E).

Interaction of *Kras*^{G12D} with expression of hair signaling pathways

One of the goals of investigating RAS gain-of-function in the hair and skin was to identify the dose-sensitive relationship between growth factor signaling and developmental pathways. The downregulation of hair matrix gene expression could reflect one or more signaling pathways that are sensitive to RAS activation and that are known to participate in hair morphogenesis, including Bone morphogenetic protein (BMP), Ectodysplasin (EDA), FGF, Hedgehog (HH), WNT, and Notch (Fig. 6A)(Schneider et al., 2009). Microarray analysis and real-time PCR of 19 genes representative of transcriptional targets or critical ligands of six pathways using microarray data and real-time PCR results suggested a number of RAS-sensitive pathways (Fig. 6B, C). However, whether these changes in *Msx2*-cre; *Kras*^{G12D} mice reflect secondary change to due the altered development of the hair follicle could not be determined. To address these issues, we utilized a skin explant assay to model physiologic RAS activation, e.g. growth factor treatment, and to identify the acute transcriptional response of the skin (Suppl. Fig. S3). Among several candidate pathways, the level and statistical significance of *Shh* RNA modulation by FGF2 was most prominent. Within 90 minutes of FGF2 stimulation, *Shh* RNA levels were reduced up to 2.8 fold, $P=2x10^{-5}$ (Suppl. Fig. S2). The acute response in wildtype explants suggested that the relationship between RTK signaling and *Shh* regulation may be direct.

Microarray data also corroborated the significance of *Shh* changes *in vivo* as several Hedgehog-related targets, including *Shh*, *Ptch1*, *Ptch2* and *Foxe1* were also downregulated in *Msx2*-cre; *Kras*^{G12D} mice (Fig. 7A) (Brancaccio et al., 2004; Tabata and Kornberg, 1994). Confirmation by quantitative real-time RT-PCR revealed a 3.78-fold reduction in *Shh* mRNA and a 2.17-fold reduction in its target gene, *Ptch1* in *Msx2*-cre*; Kras*^{G12D} skin (Fig. 7B, Suppl. Fig. S4). The reduced expression of transcriptional targets of the Hedgehog pathway indicated that in addition to reduced ligand expression, activation of the Hedgehog pathway was also reduced. To determine if reduced *Shh* levels affect the expression pattern of *Shh* in the *Msx2*-cre*; Kras*^{G12D} hair follicles, *in situ* hybridization was performed (Fig. 7C). The domain of *Shh* expression was essentially normal in *Msx2*-cre*; Kras*^{G12D} hair follicles but had reduced staining compared to wildtype hair follicles. The reduction of Hedgehog target genes suggested the reduction or inhibition of SHH ligand. Western analysis revealed ~25% reduction of mature SHH protein (Fig. 7D). Thus, *ex vivo* RTK stimulation and RAS gain-of-function *in vivo* repress cutaneous *Shh* levels.

Ex vivo effects of RAS inhibition and RTK stimulation on *Shh* transcription

The above findings suggest that use of FGF in explant studies recapitulate some aspects of *Shh* dysregulation in *Msx2*-cre*; Kras*^{G12D} hair follicles. To further localize the response of *Shh* to a component of RAS/MAPK signaling pathway, we examined the effect of inhibition of RAS effector pathways. Treatment of explants with inhibitors against downstream components of the RAS/MAPK pathway, c-RAF1 (GW5074; Lackey et al., 2000) or MEK (U0126; Favata et al., 1998), caused an increase in *Shh* mRNA levels (Fig. 8A). Treatment with a PI-3-kinase inhibitor (LY294002; Vlahos et al., 1994) also resulted in increased *Shh* mRNA levels. These studies provide further evidence that downstream effectors of RAS, i.e. MEK, RAF and PI-3-kinase, participate in the regulation of *Shh*.

We also reasoned that if *Shh* downregulation is RAS-mediated then the *Shh* response should be broadly induced by multiple receptor tyrosine kinase (RTK) signals. Thus, the response of *Shh* to epidermal growth factor (EGF), platelet-derived growth factor (PDGF), and additional FGFs (FGF7, FGF10) was also examined (Fig. 8B). Each growth factor

demonstrated a similar downregulation of *Shh* mRNA. Thus, in a wildtype hair follicle, RTK activation or inhibition of RAS downstream effector pathways both elicit rapid changes in *Shh* levels.

The rapid loss of *Shh* mRNA in the presence of FGF2 could be explained by a short intrinsic half-life of *Shh* mRNA or by FGF-induced destabilization of *Shh* mRNA. Since the half-life of *Shh* mRNA is unknown, we characterized the kinetics of *Shh* mRNA loss after pharmacologic inhibition of global transcription (Fig. 8C). Treatment of explants with actinomycin resulted in rapid decay of *Shh* mRNA, revealing an intrinsically short half-life. Furthermore, non-linear best-fit modeling showed no significant change in the *Shh* RNA half-life of FGF2 vs. actinomycin-treated explants (4.6 vs. 4.3 minutes, respectively, R^2>0.98). These findings suggest that FGF represses *Shh* mRNA levels by inhibiting transcription. To determine if transcriptional repression is responsible for decreased *Shh* mRNA in *Msx2*-cre*; Kras*^{G12D} skin, the levels of primary transcript of *Shh* RNA was evaluated (Fig. 8D). Since primary transcripts are unspliced, primers against introns 1–2, 2–3, and proximal regions of the first exon of *Shh* were generated to detect the primary transcripts of *Shh* RNA. Like its mature *Shh* mRNA, the primary transcripts of *Shh* were decreased in *Msx2*-cre; *Kras*^{G12D} mice. These findings indicate that the *Shh* mRNA is short-lived and transcriptionally repressed by growth factor signaling.

An endogenous RTK regulates *Shh* levels *in vivo*

The above studies suggested that RAS plays a role in *Shh* regulation. However, because RAS activation responds to many types of cellular signals, whether endogenous growth factor ligands participate in *Shh* transcriptional regulation in the hair follicle is unknown. In explant studies, we observed that several growth factor ligands were capable of repressing *Shh* RNA levels. FGF ligands play multiple roles in hair development, including regulation of hair growth, length determination, and medulla formation, and were ideal candidates for normal regulators of hair follicle *Shh* levels (Schlake, 2007). FGF ligands bind to one of four FGF receptors (FGFR) and activate their receptors in complex with heparan sulfate proteoglycans (Yayon et al., 1991). All four FGFRs are expressed in the hair follicle (Rosenquist and Martin, 1996). Mouse knockout studies reveal that *Fgfr3* and *Fgfr4* are not required for normal morphogenesis of the hair follicle (Deng et al., 1996; Weinstein et al., 1998). Roles of *Fgfr1* and *Fgfr2* in the hair follicle have been tested through tissue-specific inactivation and have demonstrated their roles in early formation of the hair and later in the maintenance of the hair follicle unit (Grose et al., 2007; Yang et al., 2010), but their role in ectodermal *Shh* regulation is unknown.

FGF7 and FGF10 selectively bind to ectodermal isoforms of FGFR1 and FGFR2 and are sufficient to downregulate *Shh* levels in explants (cf. Fig. 8B). Specifically, we wished to study the transcriptional response of *Shh* in the absence of *Fgfr2* in the same tissue domains as *Msx2*-cre; *Kras*^{G12D} mice (Fig. 9). *Msx2*-cre; *Fgfr2*^{flox}/− mice (*Msx2*-cre; *Fgfr2*^{cKO}) were thus generated. These mice displayed limb defects as previously reported (Yu and Ornitz, 2008) but had normal skin and hair until two weeks of age. After two weeks, the hair from *Msx2*-cre; *Fgfr2*^{cKO} mice became long, shiny and brittle, but the overall density was normal (see below). Thus, in order to study the response of *Shh* RNA to the loss of *Fgfr2*, we assayed *Shh* mRNA levels at P7 prior to the onset of these abnormalities. We detected *Shh* at more than 2-fold higher levels in *Msx2*-cre; *Fgfr2*^{cKO} mice relative to littermate controls, which included three genotypes, *Msx2*-cre; *Fgfr2*^{flox}/+, *Fgfr2*^{flox}/−, and *Fgfr2*^{flox}/+ (Fig. 9A, Suppl. Fig S4 and not shown). Increased levels of *Shh* mRNA were also accompanied by increased expression of downstream genes, *Ptch1*, *Ptch2*, *Hhip1*, and *Gli1*, indicating that Hedgehog signaling was increased in the *Msx2*-cre; *Fgfr2*^{cKO} skin.

During normal hair follicle growth, *Shh* is expressed by a transient migrating population of cells, which begins near the hair matrix. As these cells move distally, they abruptly lose *Shh* expression and eventually acquire an IRS or cuticle cell fate (Greco et al., 2009). Ectopic or persistent expression of *Shh* might also result in increased *Shh* levels in the whole skin of *Msx2*-cre; $Fgfr2^{cKO}$ mice. The negative feedback loop involving KRAS and *Shh* transcription suggest that growth factor signals might regulate the pattern or magnitude of *Shh* expression in the hair follicle. RNA *in situ* hybridization was performed on *Msx2*-cre; $Fgfr2^{cKO}$ skin to distinguish between these possibilities (Fig. 9B). *In situ* hybridization studies revealed that the overall expression pattern of *Shh* was unchanged in the absence of *Fgfr2*. A comparison of the number of *Shh*-positive cells in wildtype, *Msx2*-cre; $Fgfr2^{cKO}$, and *Msx2*-cre; $Kras^{G12D}$ hair follicles revealed no significant difference in their numbers (P= 0.4187 and P=0.4355) (Fig. 9C). To verify whether loss of ectodermal *Fgfr2* was sufficient to block acute *Shh* downregulation *ex vivo*, *Msx2*-cre; $Fgfr2^{cKO}$ explants were treated with FGF2 (Fig. 9D). There was a small but significant response of *Shh* transcription to FGF2 in the *Msx2*-cre; $Fgfr2^{cKO}$ skin, which indicating the presence of some residual functional FGFR activity. Thus, increased *Shh* mRNA levels in *Msx2*-cre; $Fgfr2^{cKO}$ skin arise independently of ectopic *Shh* expression (Fig. 9E).

DISCUSSION

In this study, hair morphogenesis was used as a model to study the developmental response to *RAS* gain-of-function. We found that in addition to the induction of a growth factor-responsive pathways, the $Kras^{G12D}$ allele also causes the downregulation of *Shh*. Downregulation of *Shh* appears to be a normal response to growth factor signaling in the hair follicle as verified through *in vitro* studies and genetic loss of FGFR2 signaling.

The hair follicle is sensitive to gain-of-function *RAS* mutations. In humans, hair shape and growth changes are prevalent in patients with germline *HRAS*, *KRAS*, *BRAF*, *MEK1*, or *MEK2* (Roberts et al., 2006). In the mouse, we find that *Kras* gain-of-function affects hair formation in multiple ways. $Kras^{G12D}$ alters hair length, features of the hair shaft, and as described previously, hair cycling (Mukhopadhyay et al., 2011). Altered proliferation in the Msx2-*cre;* $Kras^{G12D}$ hair follicle may contribute to many of the observed hair defects. Proliferation in the hair matrix is linked to the growth rate of the hair shaft. In addition, changes in proliferation are associated with altered appearance of the hair shaft including effects on hair bends in mice (Weger and Schlake, 2005). which is consistent with reduced hair growth and may further contribute to reduced numbers of medullary column and bend formation. $Kras^{G12D}$ may also have independent effects of the above characteristics as phenotypic changes in length, bends and medulla can independently affected in mouse genetic mutants (Sundberg, 1994; Schlake, 2007).

The use of an explant system facilitated the assessment of various growth factor signals that are normally present during hair follicle morphogenesis. The observation that several different growth factors are capable of *Shh* repression implies the activity of a common downstream signaling component. We also find that two parallel RAS downstream pathways, RAF/MAPK and PI-3-kinase, participate in *Shh* repression; further supporting the concept that a common component of growth factor signaling is a key regulator of *Shh*. We propose that RAS normally functions in the hair follicle as a mediator of FGFR2 activation to suppress *Shh*. SHH plays a major role in hair follicle growth (Chiang et al., 1999; Mill et al., 2003; St-Jacques et al., 1998), and thus, it seems feasible that hair growth defects in RAS gain-of-function mutations may result in part from decreased SHH levels. RAS gain-of-function affected additional signaling pathways in the hair follicle. How these additional signals cooperate with the suppression of *Shh* in the hair follicle and other organs in RAS/MAPK syndromes requires further investigation.

Much of the knowledge on *Shh* transcriptional regulation has focused on the complex cis-regulatory elements regulating its restrictive pattern during organogenesis (Amano et al., 2009; Epstein et al., 1999). However, little is known regarding the mechanisms that control its level of expression. In this study, we identify a rapid transcriptional response of the *Shh* promoter in response to RAS activation and inhibition. The half-life of *Shh* mRNA has not been previously reported. We find that unlike developmental signaling molecules, e.g. *fgf8* (Dubrulle and Pourquié, 2004), *Shh* mRNA has a very short half-life. The 3' untranslated region of *Shh* is AU-rich like many short-lived mRNAs but lacks classic AU-rich elements (Hau et al., 2007; Zubiaga et al., 1995). The short half-life of *Shh* mRNA allows for highly regulated patterns of *Shh* expression in developing organs, where cells transiently occupy signaling centers. The short half-life of *Shh* places significant reliance on transcriptional mechanisms to achieve high steady state levels of *Shh* mRNA. We find evidence that regulation of *Shh* by FGF and RAS signaling play important role in regulating the amplitude of *Shh* expression but appears to be distinct from regulatory mechanisms that regulate *Shh* pattern (cf. Fig 9E). Increased expression of morphogens by expansion of the expression domain often have deleterious effects on the morphogenesis of an organ (Oro et al., 1997). Modulation of morphogen level or sensitivity without disturbing pattern is a possible mechanism for increasing organ growth and size without affecting its shape.

The observations from the hair follicle may not be readily generalized to other organs. For example, in the limb bud, FGFR2 signaling plays both a role in the initiation and maintenance of normal domains of *Shh* expression (Lewandoski et al., 2000) and a second role in preventing ectopic *Shh* expression in the anterior limb bud (Mao et al., 2009; Zhang et al., 2009). It is also possible that FGFR2 function changes during the dynamic period of the hair cycle, and thus we cannot rule out a later function of FGF signaling in the regulation of *Shh* pattern during other stages of hair growth. The variation in hair follicle organ size at different body sites may well depend on the scalability of *Shh* expression via FGF modulation.

The above studies reveal that hair formation, shape and growth are highly sensitive to RAS/MAPK signals and serve as an even more sensitive measure than traditional biochemical markers of RAS/MAPK activation. Further studies of hair response to RAS/MAPK gain and loss-of-function may find useful application in the clinic not only in the evaluation of congenital syndromes but also as a biomarker in cancer or response to RAS/MAPK inhibition in cancer therapy.

Supplementary Material

Refer to Web version on PubMed Central for supplementary material.

Acknowledgments

We are grateful to the following: T. Jacks (LSL-$Kras^{G12D}$), D. Ornitz ($Fgfr2^{fl/fl}$), and G. Martin and R. Maxson (*Msx2*-cre), the UCSD BIOGEM Microarray Core (microarray hybridization and scanning), C. Jamora and members of the laboratory for reagents, technical assistance and discussion. This work was supported by the NIH/NIAMS to B.Y. (AR056667), CIRM to B.Y. (RN2-00908), NIH/Ruth Kirschstein NRSA to J.B. (HL07491).

References

Amano T, Sagai T, Tanabe H, Mizushina Y, Nakazawa H, Shiroishi T. Chromosomal dynamics at the *Shh* locus: limb bud-specific differential regulation of competence and active transcription. Dev Cell. 2009; 16:47–57. [PubMed: 19097946]

Aoki Y, Niihori T, Kawame H, Kurosawa K, Ohashi H, Tanaka Y, Filocamo M, Kato K, Suzuki Y, Kure S, Matsubara Y. Germline mutations in *HRAS* proto-oncogene cause Costello syndrome. Nat Genet. 2005; 37:1038–1040. [PubMed: 16170316]

Axelrad ME, Schwartz DD, Fehlis JE, Hopkins E, Stabley DL, Sol-Church K, Gripp KW. Longitudinal course of cognitive, adaptive, and behavioral characteristics in Costello syndrome. Amer J of Med Genet Part A. 2009; 149A:2666–2672. [PubMed: 19919001]

Bertola DR, Pereira AC, Brasil AS, Albano LM, Kim CA, Krieger JE. Further evidence of genetic heterogeneity in Costello syndrome: involvement of the *KRAS* gene. J of Hum Genet. 2007; 52:521–526. [PubMed: 17468812]

Bollag G, Hirth P, Tsai J, Zhang J, Ibrahim PN, Cho H, Spevak W, Zhang C, Zhang Y, Habets G, Burton EA, Wong B, Tsang G, West BL, Powell B, Shellooe R, Marimuthu A, Nguyen H, Zhang KYJ, Artis DR, Schlessinger J, Su F, Higgins B, Iyer R, D'Andrea K, Koehler A, Stumm M, Lin PS, Lee RJ, Grippo J, Puzanov I, Kim KB, Ribas A, McArthur GA, Sosman JA, Chapman PB, Flaherty KT, Xu X, Nathanson KL, Nolop K. Clinical efficacy of a RAF inhibitor needs broad target blockade in BRAF-mutant melanoma. Nature. 2010; 467:596–599. [PubMed: 20823850]

Brancaccio A, Minichiello A, Grachtchouk M, Antonini D, Sheng H, Parlato R, Dathan N, Dlugosz AA, Missero C. Requirement of the forkhead gene *Foxe1*, a target of sonic hedgehog signaling, in hair follicle morphogenesis. Hum Mol Genet. 2004; 13:2595–2606. [PubMed: 15367491]

Chiang C, Swan RZ, Grachtchouk M, Bolinger M, Litingtung Y, Robertson EK, Cooper MK, Gaffield W, Westphal H, Beachy PA, Dlugosz AA. Essential role for *Sonic hedgehog* during hair follicle morphogenesis. Dev Biol. 1999; 205:1–9. [PubMed: 9882493]

Corson LB, Yamanaka Y, Lai KM, Rossant J. Spatial and temporal patterns of ERK signaling during mouse embryogenesis. Development. 2003; 130:4527–4537. [PubMed: 12925581]

Courtois-Cox S, Genther Williams SM, Reczek EE, Johnson BW, McGillicuddy LT, Johannessen CM, Hollstein PE, MacCollin M, Cichowski K. A negative feedback signaling network underlies oncogene-induced senescence. Cancer Cell. 2006; 10:459–472. [PubMed: 17157787]

Deng C, Wynshaw-Boris A, Zhou F, Kuo A, Leder P. Fibroblast growth factor receptor 3 is a negative regulator of bone growth. Cell. 1996; 84:911–921. [PubMed: 8601314]

Downward J. Targeting RAS signalling pathways in cancer therapy. Nat Rev. 2003; 3:11–22.

Dubrulle J, Pourquié O. *Fgf8* mRNA decay establishes a gradient that couples axial elongation to patterning in the vertebrate embryo. Nature. 2004; 427:419–422. [PubMed: 14749824]

Epstein DJ, McMahon AP, Joyner AL. Regionalization of Sonic hedgehog transcription along the anteroposterior axis of the mouse central nervous system is regulated by Hnf3-dependent and -independent mechanisms. Development. 1999; 126:281–292. [PubMed: 9847242]

Etchevers HC, Vincent C, Le Douarin NM, Couly GF. The cephalic neural crest provides pericytes and smooth muscle cells to all blood vessels of the face and forebrain. Development. 2001; 128:1059–1068. [PubMed: 11245571]

Favata MF, Horiuchi KY, Manos EJ, Daulerio AJ, Stradley DA, Feeser WS, Van Dyk DE, Pitts WJ, Earl RA, Hobbs F, Copeland RA, Magolda RL, Scherle PA, Trzaskos JM. Identification of a novel inhibitor of mitogen-activated protein kinase kinase. J Biol Chem. 1998; 273:18623–18632. [PubMed: 9660836]

Greco V, Chen T, Rendl M, Schober M, Pasolli HA, Stokes N, Dela Cruz-Racelis J, Fuchs E. A two-step mechanism for stem cell activation during hair regeneration. Cell Stem Cell. 2009; 4:155–169. [PubMed: 19200804]

Gripp KW, Hopkins E, Doyle D, Dobyns WB. High incidence of progressive postnatal cerebellar enlargement in Costello syndrome: brain overgrowth associated with *HRAS* mutations as the likely cause of structural brain and spinal cord abnormalities. Amer J Med Genet Part A. 2010; 152A:1161–1168. [PubMed: 20425820]

Grose R, Fantl V, Werner S, Chioni AM, Jarosz M, Rudling R, Cross B, Hart IR, Dickson C. The role of fibroblast growth factor receptor 2b in skin homeostasis and cancer development. EMBO J. 2007; 26:1268–1278. [PubMed: 17304214]

Hau HH, Walsh RJ, Ogilvie RL, Williams DA, Reilly CS, Bohjanen PR. Tristetraprolin recruits functional mRNA decay complexes to ARE sequences. J Cell Biochem. 2007; 100:1477–1492. [PubMed: 17133347]

Johnson L, Greenbaum D, Cichowski K, Mercer K, Murphy E, Schmitt E, Bronson RT, Umanoff H, Edelmann W, Kucherlapati R, Jacks T. *K-ras* is an essential gene in the mouse with partial functional overlap with *N-ras*. Genes Dev. 1997; 11:2468–2481. [PubMed: 9334313]

Kawakami Y, Rodriguez-Leon J, Koth CM, Buscher D, Itoh T, Raya A, Ng JK, Esteban CR, Takahashi S, Henrique D, Schwarz MF, Asahara H, Izpisua Belmonte JC. MKP3 mediates the cellular response to FGF8 signalling in the vertebrate limb. Nat Cell Biol. 2003; 5:513–519. [PubMed: 12766772]

Lackey K, Cory M, Davis R, Frye SV, Harris PA, Hunter RN, Jung DK, McDonald OB, McNutt RW, Peel MR, Rutkowske RD, Veal JM, Wood ER. The discovery of potent cRaf1 kinase inhibitors. Bioorg & Med Chem Letters. 2000; 10:223–226.

Lewandoski M, Sun X, Martin GR. *Fgf8* signalling from the AER is essential for normal limb development. Nat Genet. 2000; 26:460–463. [PubMed: 11101846]

Lewis PM, Dunn MP, McMahon JA, Logan M, Martin JF, St-Jacques B, McMahon AP. Cholesterol modification of sonic hedgehog is required for long-range signaling activity and effective modulation of signaling by Ptc1. Cell. 2001; 105:599–612. [PubMed: 11389830]

Lin AE, Alexander ME, Colan SD, Kerr B, Rauen KA, Noonan J, Baffa J, Hopkins E, Sol-Church K, Limongelli G, Digilio MC, Marino B, Innes AM, Aoki Y, Silberbach M, Delrue MA, White SM, Hamilton RM, O'Connor W, Grossfeld PD, Smoot LB, Padera RF, Gripp KW. Clinical, pathological, and molecular analyses of cardiovascular abnormalities in Costello syndrome: A Ras/MAPK pathway syndrome. Amer J Med Genet Part A. 2011; 155A(3):486–507. [PubMed: 21344638]

Malumbres M, Barbacid M. RAS oncogenes: the first 30 years. Nat Rev Cancer. 2003; 3:459–465. [PubMed: 12778136]

Mao J, McGlinn E, Huang P, Tabin CJ, McMahon AP. Fgf-dependent *Etv4/5* activity is required for posterior restriction of Sonic Hedgehog and promoting outgrowth of the vertebrate limb. Dev Cell. 2009; 16:600–606. [PubMed: 19386268]

Marshall CJ. Specificity of receptor tyrosine kinase signaling: transient versus sustained extracellular signal-regulated kinase activation. Cell. 1995; 80:179–185. [PubMed: 7834738]

Meijering E, Jacob M, Sarria JC, Steiner P, Hirling H, Unser M. Design and validation of a tool for neurite tracing and analysis in fluorescence microscopy images. Cytometry A. 2004; 58:167–176. [PubMed: 15057970]

Mill P, Mo R, Fu H, Grachtchouk M, Kim PCW, Dlugosz AA, Hui C-c. Sonic hedgehog-dependent activation of *Gli2* is essential for embryonic hair follicle development. Genes Dev. 2003; 17:282–294. [PubMed: 12533516]

Mukhopadhyay A, Krishnaswami SR, Yu BDY. Activated *Kras* alters epidermal homeostasis of mouse skin, resulting in redundant skin and defective hair cycling. J Invest Derm. 2011; 131:311–319. [PubMed: 20944652]

Murphy LO, Smith S, Chen RH, Fingar DC, Blenis J. Molecular interpretation of ERK signal duration by immediate early gene products. Nat Cell Biol. 2002; 4:556–564. [PubMed: 12134156]

Mustonen T, Pispa J, Mikkola ML, Pummila M, Kangas AT, Pakkasjarvi L, Jaatinen R, Thesleff I. Stimulation of ectodermal organ development by Ectodysplasin-A1. Dev Biol. 2003; 259:123–136. [PubMed: 12812793]

Noonan JA. Noonan syndrome and related disorders: Alterations in growth and puberty. Rev Endoc Metab Disorders. 2006; 7:251–255.

Oro AE, Higgins KM, Hu Z, Bonifas JM, Epstein EH Jr, Scott MP. Basal cell carcinomas in mice overexpressing sonic hedgehog. Science. 1997; 276:817–821. [PubMed: 9115210]

Pan Y, Lin MH, Tian X, Cheng HT, Gridley T, Shen J, Kopan R. gamma-secretase functions through Notch signaling to maintain skin appendages but is not required for their patterning or initial morphogenesis. Dev Cell. 2004; 7:731–743. [PubMed: 15525534]

Rauen KA, Schoyer L, McCormick F, Lin AE, Allanson JE, Stevenson DA, Gripp KW, Neri G, Carey JC, Legius E, Tartaglia M, Schubbert S, Roberts AE, Gelb BD, Shannon K, Gutmann DH, McMahon M, Guerra C, Fagin JA, Yu B, Aoki Y, Neel BG, Balmain A, Drake RR, Nolan GP, Zenker M, Bollag G, Sebolt-Leopold J, Gibbs JB, Silva AJ, Patton EE, Viskochil DH, Kieran MW, Korf BR, Hagerman RJ, Packer RJ, Melese T. Proceedings from the 2009 genetic syndromes

of the Ras/MAPK pathway: From bedside to bench and back. Amer J Med Genet Part A. 2010; 152A:4–24. [PubMed: 20014119]

Rendl M, Lewis L, Fuchs E. Molecular dissection of mesenchymal-epithelial interactions in the hair follicle. PLoS Biol. 2005; 3:e331–e331. [PubMed: 16162033]

Reuther GW, Der CJ. The Ras branch of small GTPases: Ras family members don't fall far from the tree. Curr Opin Cell Biol. 2000; 12:157–165. [PubMed: 10712923]

Roberts A, Allanson J, Jadico SK, Kavamura MI, Noonan J, Opitz JM, Young T, Neri G. The cardiofaciocutaneous syndrome. J Med Genet. 2006; 43:833–842. [PubMed: 16825433]

Rodriguez-Viciana P, Tetsu O, Oda K, Okada J, Rauen K, McCormick F. Cancer targets in the Ras pathway. Cold Spring Harbor Symp Quant Biol. 2005; 70:461–467. [PubMed: 16869784]

Rodriguez-Viciana P, Tetsu O, Tidyman WE, Estep AL, Conger BA, Cruz MS, McCormick F, Rauen KA. Germline mutations in genes within the MAPK pathway cause cardio-facio-cutaneous syndrome. Science. 2006; 311:1287–1290. [PubMed: 16439621]

Rodriguez-Viciana P, Warne PH, Khwaja A, Marte BM, Pappin D, Das P, Waterfield MD, Ridley A, Downward J. Role of phosphoinositide 3-OH kinase in cell transformation and control of the actin cytoskeleton by Ras. Cell. 1997; 89:457–467. [PubMed: 9150145]

Rosenquist TA, Martin GR. Fibroblast growth factor signalling in the hair growth cycle: expression of the fibroblast growth factor receptor and ligand genes in the murine hair follicle. Dev Dyn. 1996; 205:379–386. [PubMed: 8901049]

Schlake T. Determination of hair structure and shape. Sem Cell Dev Biol. 2007; 18:267–273.

Schneider MR, Schmidt-Ullrich R, Paus R. The hair follicle as a dynamic miniorgan. Curr Biol. 2009; 19:R132–142. [PubMed: 19211055]

Schubbert S, Zenker M, Rowe SL, Boll S, Klein C, Bollag G, van der Burgt I, Musante L, Kalscheuer V, Wehner LE, Nguyen H, West B, Zhang KY, Sistermans E, Rauch A, Niemeyer CM, Shannon K, Kratz CP. Germline *KRAS* mutations cause Noonan syndrome. Nat Genet. 2006; 38:331–336. [PubMed: 16474405]

Schweitzer R, Shilo BZ. A thousand and one roles for the Drosophila EGF receptor. Trends Genet. 1997; 13:191–196. [PubMed: 9154002]

Siegel DH, Mann JA, Krol AL, Rauen KA. Dermatological phenotype in Costello syndrome: consequences of Ras dysregulation in development. Br J Dermatol. 2012; 166:601–607. [PubMed: 22098123]

Siegel DH, McKenzie J, Frieden IJ, Rauen KA. Dermatological findings in 61 mutation-positive individuals with cardiofaciocutaneous syndrome. Br J Dermatol. 2011; 164:521–529. [PubMed: 21062266]

St-Jacques B, Dassule HR, Karavanova I, Botchkarev VA, Li J, Danielian PS, McMahon JA, Lewis PM, Paus R, McMahon AP. Sonic hedgehog signaling is essential for hair development. Curr Biol. 1998; 8:1058–1068. [PubMed: 9768360]

Sun X, Lewandoski M, Meyers EN, Liu YH, Maxson RE, Martin GR. Conditional inactivation of *Fgf4* reveals complexity of signalling during limb bud development. Nat Genet. 2000; 25:83–86. [PubMed: 10802662]

Sundberg, J. Handbook of mouse mutations with skin and hair abnormalities : animal models and biomedical tools. CRC Press; Boca Raton: 1994.

Tabata T, Kornberg TB. Hedgehog is a signaling protein with a key role in patterning Drosophila imaginal discs. Cell. 1994; 76:89–102. [PubMed: 8287482]

Tidyman WE, Rauen KA. The RASopathies: developmental syndromes of Ras/MAPK pathway dysregulation. Curr Opin Genet Dev. 2009; 19:230–236. [PubMed: 19467855]

Tuveson DA, Shaw AT, Willis NA, Silver DP, Jackson EL, Chang S, Mercer KL, Grochow R, Hock H, Crowley D, Hingorani SR, Zaks T, King C, Jacobetz MA, Wang L, Bronson RT, Orkin SH, DePinho RA, Jacks T. Endogenous oncogenic K-ras(G12D) stimulates proliferation and widespread neoplastic and developmental defects. Cancer Cell. 2004; 5:375–387. [PubMed: 15093544]

Verheyden JM, Lewandoski M, Deng C, Harfe BD, Sun X. Conditional inactivation of *Fgfr1* in mouse defines its role in limb bud establishment, outgrowth and digit patterning. Development. 2005; 132:4235–4245. [PubMed: 16120640]

Vlahos CJ, Matter WF, Hui KY, Brown RF. A specific inhibitor of phosphatidylinositol 3-kinase, 2-(4-morpholinyl)-8-phenyl-4H-1-benzopyran-4-one (LY294002). J Biol Chem. 1994; 269:5241–5248. [PubMed: 8106507]

Weger N, Schlake T. Igf-I signalling controls the hair growth cycle and the differentiation of hair shafts. The Journal of investigative dermatology. 2005; 125:873–882. [PubMed: 16297183]

Weinstein M, Xu X, Ohyama K, Deng CX. FGFR-3 and FGFR-4 function cooperatively to direct alveogenesis in the murine lung. Development. 1998; 125:3615–3623. [PubMed: 9716527]

Weinstein M, Xu X, Ohyama K, Deng CX. FGFR-3 and FGFR-4 function cooperatively to direct alveogenesis in the murine lung. Development. 1998; 125:3615–3623. [PubMed: 9716527]

Yang J, Meyer M, Müller AK, Böhm F, Grose R, Dauwalder T, Verrey F, Kopf M, Partanen J, Bloch W, Ornitz DM, Werner S. Fibroblast growth factor receptors 1 and 2 in keratinocytes control the epidermal barrier and cutaneous homeostasis. J Cell Biol. 2010; 188:935–952. [PubMed: 20308431]

Yayon A, Klagsbrun M, Esko JD, Leder P, Ornitz DM. Cell surface, heparin-like molecules are required for binding of basic fibroblast growth factor to its high affinity receptor. Cell. 1991; 64:841–848. [PubMed: 1847668]

Yekutieli D, Benjamini Y. The control of the false discovery rate in multiple testing under dependency. Annals Stat. 2001; 29:1165–1188.

Yu K, Ornitz DM. FGF signaling regulates mesenchymal differentiation and skeletal patterning along the limb bud proximodistal axis. Development. 2008; 135:483–491. [PubMed: 18094024]

Yu K, Xu J, Liu Z, Sosic D, Shao J, Olson EN, Towler DA, Ornitz DM. Conditional inactivation of FGF receptor 2 reveals an essential role for FGF signaling in the regulation of osteoblast function and bone growth. Development. 2003; 130:3063–3074. [PubMed: 12756187]

Zenker M, Lehmann K, Schulz AL, Barth H, Hansmann D, Koenig R, Korinthenberg R, Kreiss-Nachtsheim M, Meinecke P, Morlot S, Mundlos S, Quante AS, Raskin S, Schnabel D, Wehner LE, Kratz CP, Horn D, Kutsche K. Expansion of the genotypic and phenotypic spectrum in patients with *KRAS* germline mutations. J Med Genet. 2007; 44:131–135. [PubMed: 17056636]

Zhang Z, Verheyden JM, Hassell JA, Sun X. FGF-regulated *Etv* genes are essential for repressing Shh expression in mouse limb buds. Dev Cell. 2009; 16:607–613. [PubMed: 19386269]

Zubiaga, AM.; Belasco, JG.; Greenberg, ME. The nonamer UUAUUUAUU is the key. 1995.

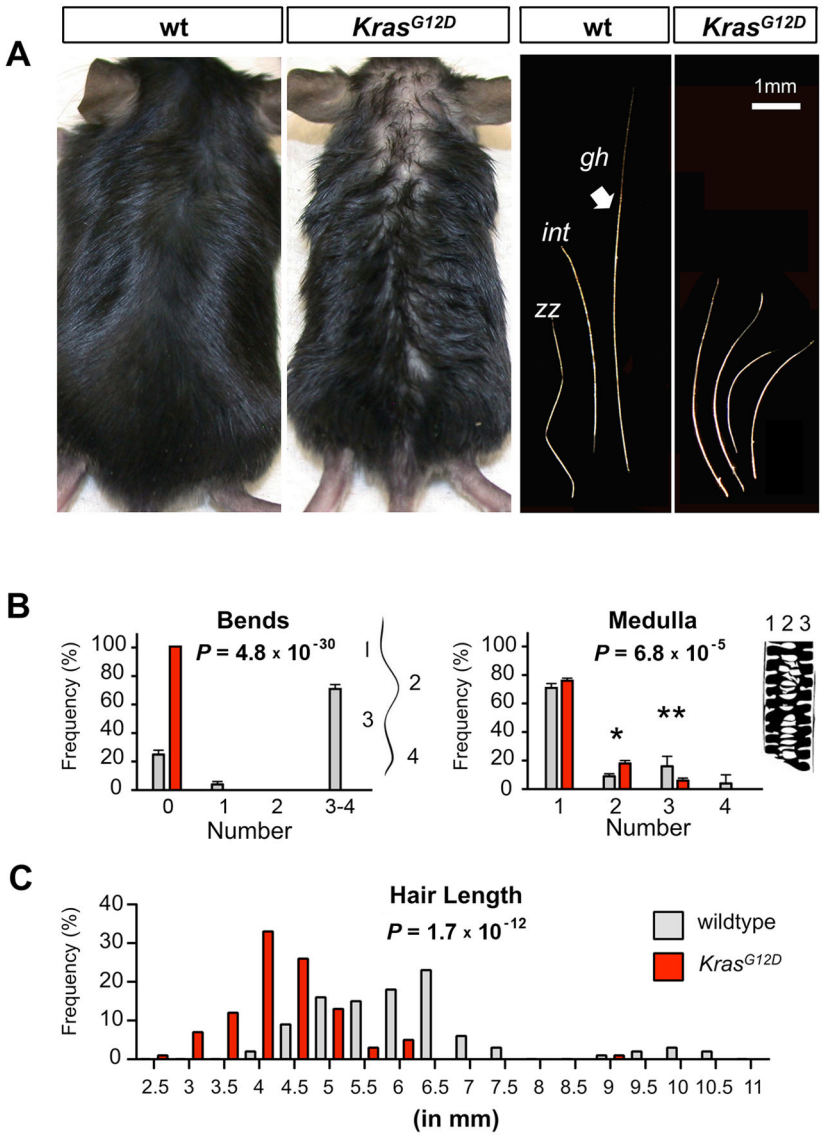

Figure 1. Hair analysis of wildtype and Msx2-*cre; Kras*^{G12D} gain-of-function mice

(A) (Left panels) P14 wildtype (wt) and Msx2-*cre; Kras*^{G12D} *(Kras*^{G12D}*)* mice and (right panels) darkfield micrographs of hair shaft morphology. Wildtype mice demonstrate characteristic guard (gh), intermediate awl/auchene (int), and zigzag (zz) hair types. *Kras*^{G12D}-hair shafts were short, curved and lacked hair bends. Scale bar = 1 mm. (B) Frequency of hair with hair bends (left panel) and with varying numbers of medulla columns (right panel) in wildtype and *Kras*^{G12D} mice. Tracing of representative hair shaft at low power demonstrating four bends and, at higher power, demonstrating three medulla columns. Single asterisk (*), P=0.003; double asterisks (**), P=0.009. (C) Frequency of hair of varying lengths in wildtype and *Kras*^{G12D} mice. Data represents > 100 hair shafts from at least three animals of each genotype with a mean hair length of 5.98 and 4.11 mm in wildtype and *Kras*^{G12D} mice, respectively (P<0.0001).

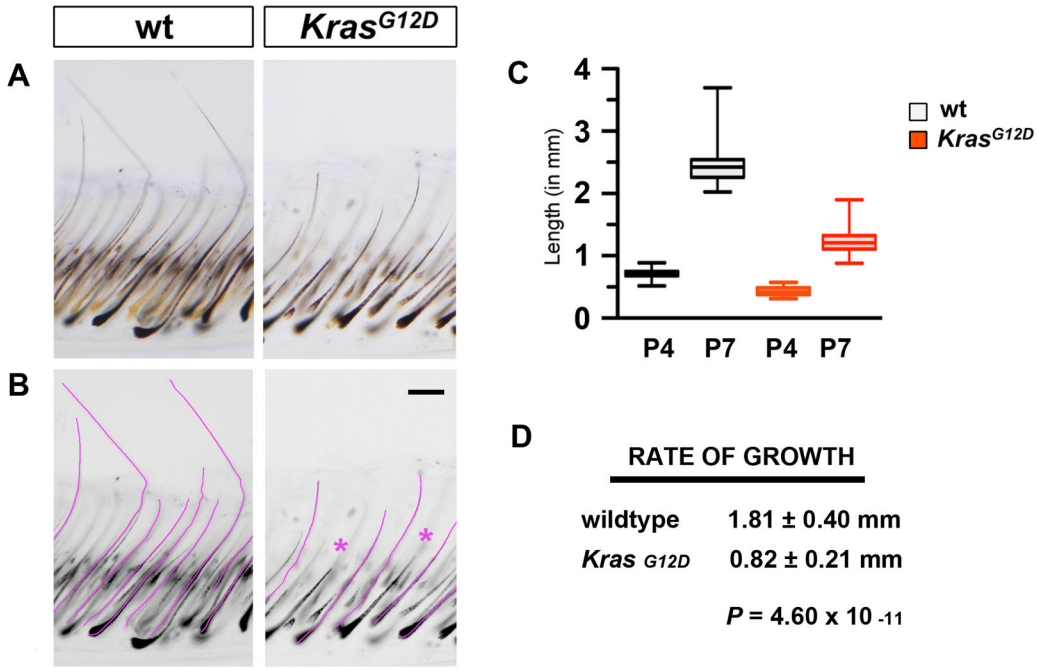

Figure 2. Growth of hair follicles in wildtype and Msx2-*cre; Kras*^{G12D} mice

(A) Cleared P4 whole skin of wildtype and Msx2-*cre; Kras*^{G12D} mice, demonstrating hair shaft and hair follicles. (B) Tracings of example complete hair shaft and follicles from cleared P4 skin. Asterisks indicate broken hair shafts, which were excluded from analysis. Scale bar =100 μm. (C) Plot of average length of P4 vs. P7 hair shafts from wildtype and Msx2-*cre; Kras*^{G12D} mice, representing at least four mice per age. (D) Summary of change in hair length between P4 and P7 in wildtype and Msx2-*cre; Kras*^{G12D} mice and statistical significance.

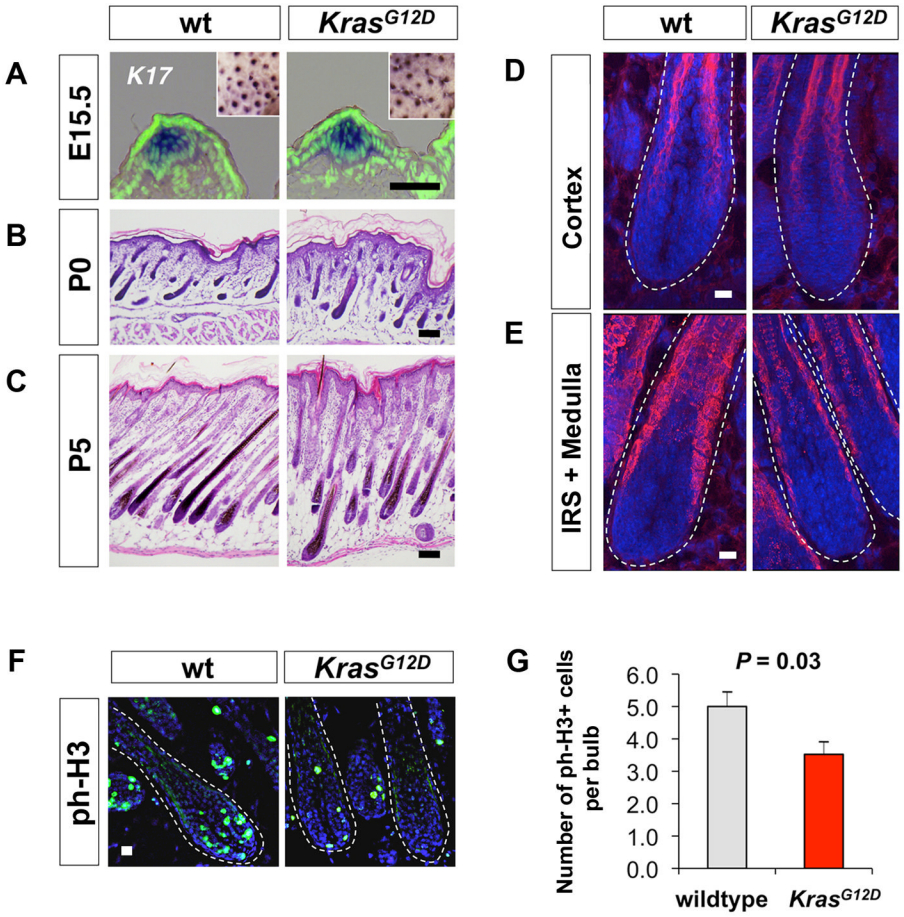

Figure 3. Appearance, proliferation, differentiation of Msx2-*cre; Kras*^{G12D} hair follicles

(A) Placode morphology and density (inset) at E15.5 revealed by keratin 17 (K17) RNA *in situ* hybridization in wildtype and Msx2-cre; *Kras*^{G12D} (*Kras*^{G12D}) embryos. Sections are counterstained with Sytox Green. Scale bar = 200 μm. (B, C) Histology of P0 and P5 hair follicles demonstrating similar hair follicle density and maturation in wildtype and *Kras*^{G12D} mice. At P5, *Kras*^{G12D} hair follicles begin to demonstrate abnormal orientation. Scale bars = 500 μm. (D, E) Immuno-fluorescent analysis of hair differentiation in wildtype and *Kras*^{G12D} P7 hair follicles. Hair keratin (AE13)-positive staining delineates hair cortical and cuticle cells, which are present in both wildtype and *Kras*^{G12D} mutant skin. Trichohyalin (AE15)-positive staining reveals internal hair medulla cells in addition to supporting IRS cells. Scale = 20 μm. (F, G) Mitotic index determined by phospho-histone H3 (ph-H3) staining on P7 wildtype and *Kras*^{G12D} mutant hair follicles. Numbers of ph-H3-positive cells per hair bulb were determined for both genotypes. Scale = 20 μm.

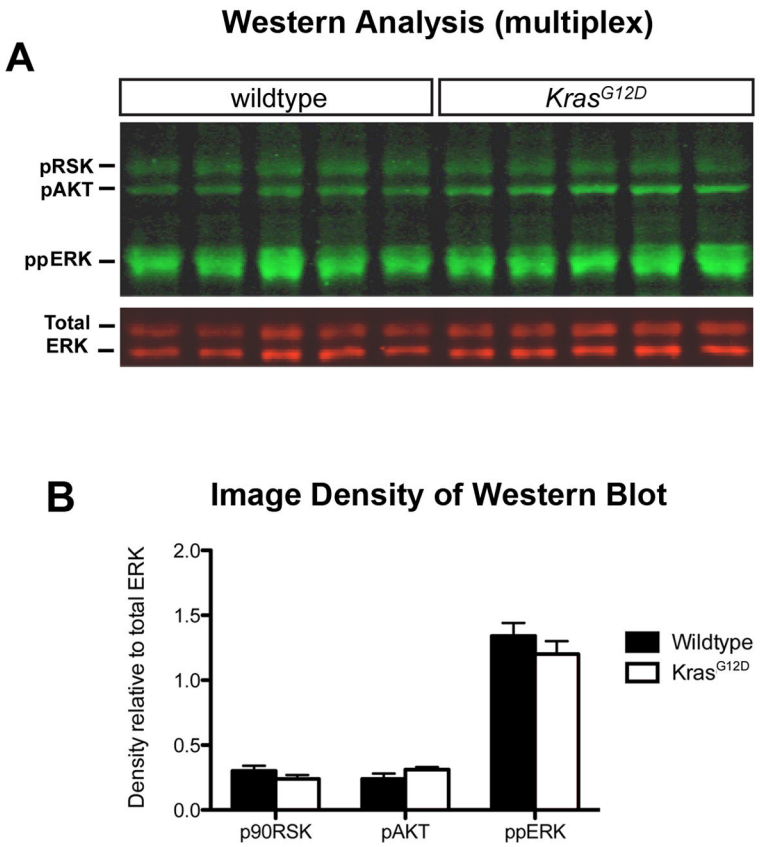

Figure 4. Biochemical and transcriptional response of skin to *Kras*^{G12D}

(A) Immunoblot analysis of phosphorylated downstream effector proteins (green) in wildtype and *Kras*^{G12D} P4 skin. Samples show no significant change after normalized with total ERK (red), which also serves as a loading control. (B) Densitometry analysis of phosphorylated p90RSK, AKT, and ERK normalized to total ERK show no significant change of whole skin at baseline

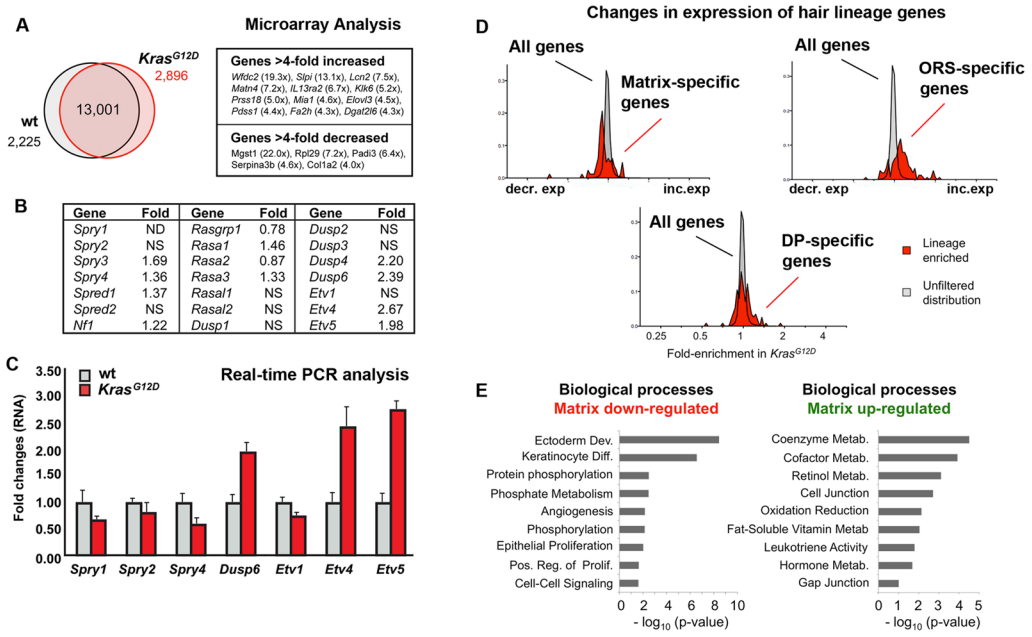

Figure 5. Microarray analysis of cutaneous response to *Kras^{G12D}*

(A) Venn diagram of altered gene expression (P<0.05) and table (4x change) summarizing differential gene expression and potential *Kras^{G12D}* biomarkers from microarray analysis, 13,001 genes noted in intersection of Venn diagram indicate number of genes that are not significantly altered between biological triplicates. (B) Effect of *Kras^{G12D}* on the expression of previously reported biomarkers of RAS activation and growth factor signaling. NS, not statistically significant; ND, not detected. (C) Quantitative real-time PCR validation of RAS/growth factor signaling biomarkers confirms increased expression of *Dusp6, Etv4,* and *Etv5.* (D) Effect of *Kras^{G12D}* on expression of hair matrix, ORS, and dermal papilla (OP)-specific genes (red area curve). Normal distribution of gene expression is shown in gray. (E) Biological processes and P- values (negative $\log_{10}$) of association reflected in gene expression as predicted by Gene Ontology.

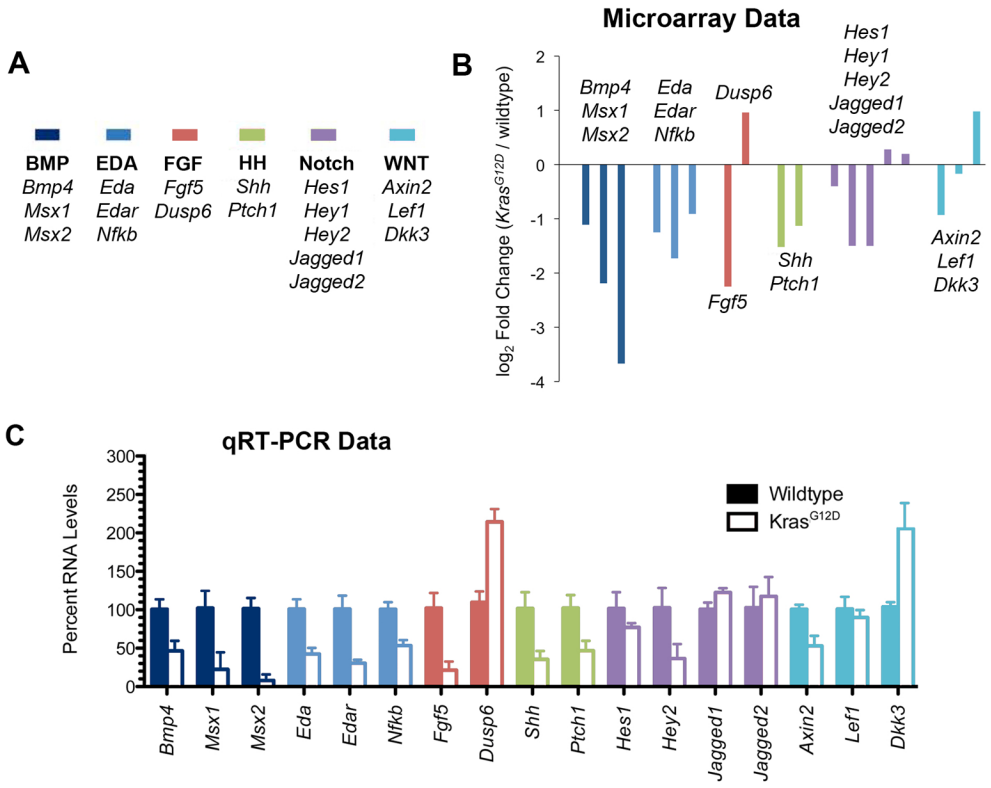

Figure 6. Effect of *Kras*^{G12D} on cutaneous expression of candidate morphogen pathways

(A) Legend for selected target genes tested and their association with candidate morphogen pathways. (B) Microarray data for genes representing morphogen pathways, demonstrating relative changes in gene expression in *Kras*^{G12D} / wildtype. (C) Real-time PCR analysis of genes of morphogen pathways of P7 whole skin from wildtype (solid) and *Kras*^{G12D} (unfilled) mice.

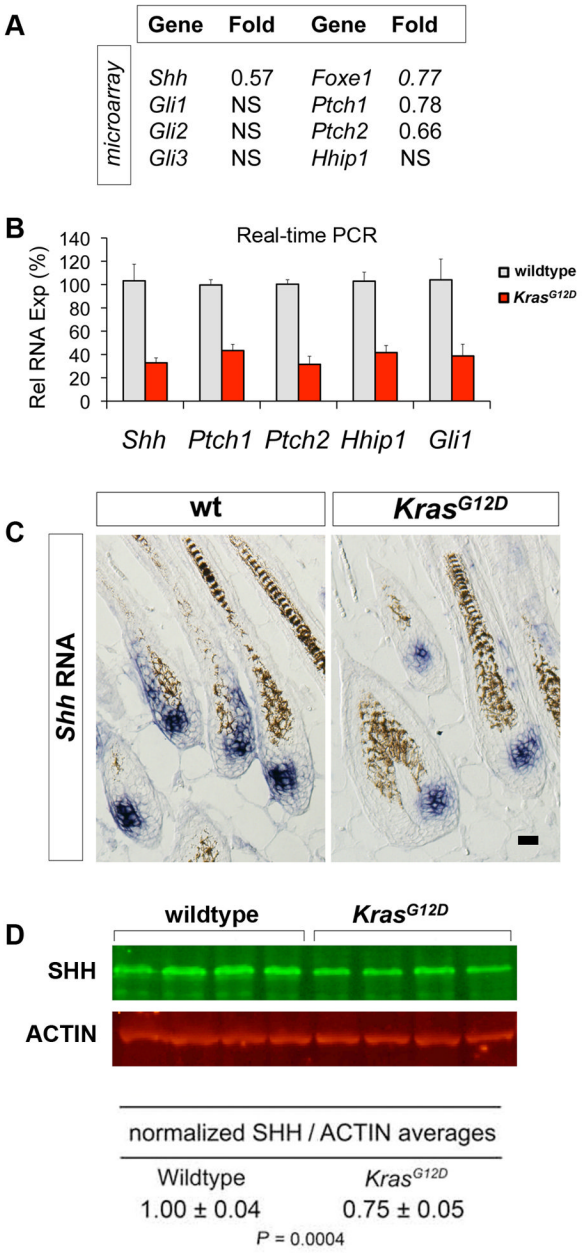

Figure 7. Effect of *Kras*^{G12D} on cutaneous Hedgehog signaling

(A) Microarray analysis of genes within the Hedgehog signaling pathway demonstrates decreased *Shh* in addition to three downstream targets, *Foxe1*, *Ptch1*, and *Ptch2*. NS, no significant change. (B) Real-time PCR of analysis of Hedgehog pathway genes (*Shh*, *Ptch1*, *Ptch2*, *Hhip1*, and *Gli1* RNA) from P7 wildtype and *Kras*^{G12D} whole skin (n=4 of each genotype). (C) *In situ* hybridization for *Shh* RNA in P7 wildtype and Msx2-*cre; Kras*^{G12D} skin show similar patterns of expression in hair follicle. (D) Western blot of SHH protein (green) and ACTIN loading control (red) for four animals of each genotype. Summary of image densitometry analysis indicates ~25% reduction in SHH protein.

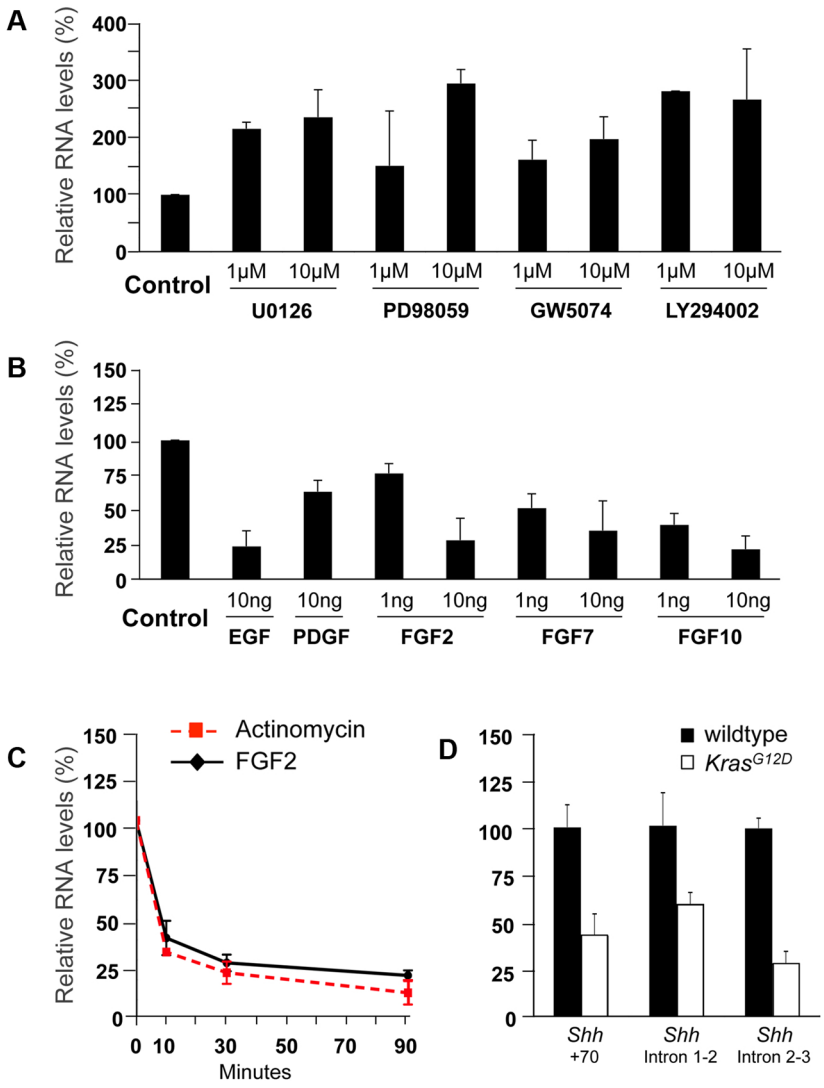

Figure 8. Cutaneous *Shh* regulation in wildtype skin in response to growth factor stimulation or RAS/MAPK inhibition

(A) *Shh* RNA explant levels following 90-minute inhibitor treatment with U0126 (MEK1/2), PD98059 (MEK1), GW5074 (c-RAF), and LY294002 (PI-3-kinase). (B) *Shh* RNA explant levels in response to 90-minute treatment with EGF, PDGF, FGF2, FGF7 and FGF10. Explant results (A and B) reflect at least three control animal studies. (C) Similar kinetics of *Shh* RNA downregulation in response to FGF2 or actinomycin (red dashed line) relative to control treated skin explants. (D) Levels of *Shh* unspliced primary transcript are reduced in the skin of Msx2-*cre; Kras*^{G12D} mice relative to wildtype as detected by proximal exon (+70) and two downstream introns.

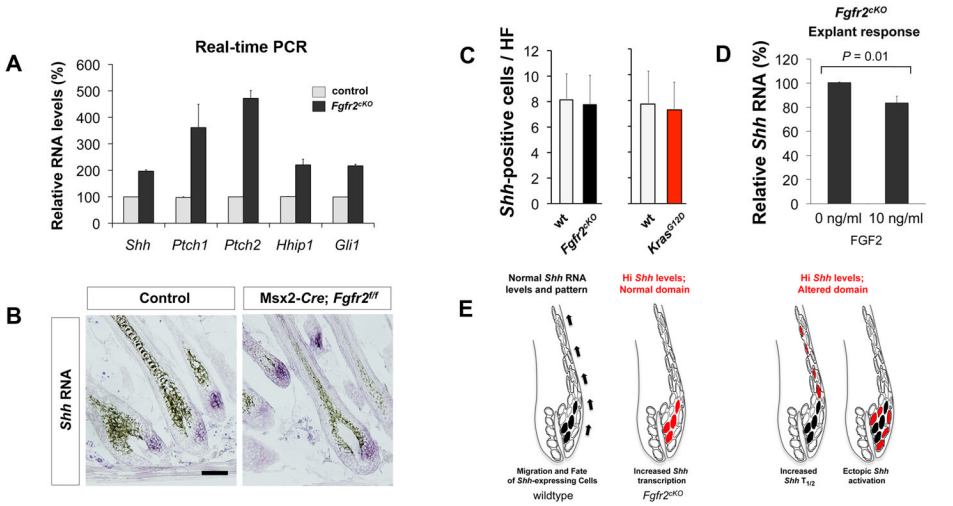

Figure 9. Genetic loss of *Fgfr2* is associated with increased *Shh* gene expression

(A) Real-time PCR analysis of Hedgehog pathway gene expression *(Shh, Ptch1, Ptch2, Hhip1* and *G1i1)* in wildtype and Msx2-*cre; Fgfr2*^{CKO} *(Fgfr2*^{CKO}*)* P7 mouse whole skin. (B) *In situ* hybridization of *Shh* RNA (purple) in wildtype and *Fgfr2*^{CKO} mouse skin. Black granules are melanin. (C) Average numbers of *Shh*-positive cells in hair bulb region of *Fgfr2*^{CKO}, *Kras*^{G12D} and wildtype littermates. At least three animals were used in these studies and statistical differences between mutant and wildtype littermates were P=0.4187 and P=0.4355 for *Fgfr2*^{CKO} and *Kras*^{G12D}, respectively. (D) Relative resistance of *Shh* downregulation by FGF2 in *Fgfr2*^{CKO} P7 explants. Relative levels of *Shh* RNA are shown in *Fgfr2*^{CKO} explants +/− 90-minute treatment with FGF2.

(E) The schematic depicts the pattern of *Shh* expression under normal conditions (black shading) or conditions in which overall *Shh* levels are increased (red shading). In Msx2-*cre; Fgfr2*^{CKO} mice, *Shh* levels are increased its normal expression domain rather than by ectopic *Shh* expression.